

HYBRID INTEGRATED NANOPHOTONIC SILICON-BASED STRUCTURES

THI HONG CAM HOANG^{1,2}, THANH BINH PHAM², THUY VAN NGUYEN²,
VAN DAI PHAM², HUY BUI², VAN HOI PHAM², ELENA DURAN³, CARLOS RAMOS³,
XAVIER LE ROUX³, LAURENT VIVIEN³ AND ERIC CASSAN³

¹*University of Science and Technology of Hanoi,
Vietnam Academy of Science and Technology, 18 Hoang Quoc Viet, Cau Giay, Hanoi, Vietnam*

²*Institute of Materials Science,
Vietnam Academy of Science and Technology, 18 Hoang Quoc Viet, Cau Giay, Hanoi, Vietnam*

³*Centre for Nanoscience and Nanotechnology, CNRS, Université Paris-Sud,
Université Paris-Saclay, 10 Boulevard Thomas Gobert, 91120 Palaiseau, France*

†*E-mail: hoang-thi-hong.cam@usth.edu.vn*

Received 3 June 2019

Accepted for publication 30 November 2019

Published 12 December 2019

Abstract. *We report nanophotonic silicon-based devices for hybrid integration: 1D photonic crystal (PhC) on optical fiber, i. e. fiber Bragg grating (FBG) sensing probe integrated in fiber laser structure for chemical sensors and slotted planar 2D PhC cavity combined with carbon nanotube (CNT) towards light nanosources. The experiments have been carried out by integrating 1D PhC on optical fiber in fiber laser structure. This structure possesses many advantages including high resolution for wavelength shift, high optical signal-to-noise ratio (OSNR) of about 50 dB, the small full width at half-maximum (FWHM) of about 0.014 nm therefore its accuracy is enhanced, as well as the precision and capability are achieved for remote sensing. Low nitrate concentration in water from 0 to 80 ppm has been used to demonstrate its sensing ability in the experiment. The proposed sensor can work with good repeatability, rapid response, and its sensitivity can be obtained of 3.2×10^{-3} nm/ppm with the limit of detection (LOD) of 3 ppm. For 2D PhC cavity, enhancement of photoluminescence of CNT emission is observed. The semiconducting single-walled carbon nanotubes (s-SWNTs) solution was prepared by polymer-sorted method and coupled with the confined modes in silicon slotted PhC cavities. The enhancement ratio of 1.15 is obtained by comparing between the PL peaks at two confined modes of the cavity. The PL enhancement result of the integrated system shows the potential for the realization of on-chip nanoscale sources.*

Keywords: nanophotonic devices; fiber Bragg grating; photonic crystal.

Classification numbers: 42.55.tv; 42.81.-i.

I. INTRODUCTION

Nanophotonics – the study of the behavior of light on the nano scale, and of the interaction of nanometer-scale objects with light – has been emerging in many applications, including optical interconnects, wavelength division multiplexing (WDM) systems, modulators, light nanosources, sensing, etc. The progress of technology as well as the development of new materials are crucial for the realization of nanophotonic structures. The common semiconductors used in nanophotonics can be listed as III-V direct bandgap semiconductor such as GaAs [1, 2] or group IV semiconductor, *e.g.* silicon which are well compatible with Complementary Metal-Oxide-Semiconductor (CMOS) technology. Silicon photonics has now played a dominant role in photonic technology [3]. In group IV silicon photonics, photonic crystal (PhC) structures [4–6] have been widely exploited in order to take the benefit from slow-light mode in such a periodic modulation geometry of the refractive index [7]. With the band gaps from dielectric lattices, PhCs are of great interest for applications in optical sensors [8], multi/demultiplexers [9], quantum information processing [10]. These structures including 1-dimensional (1D), 2-dimensional (2D) and 3-dimensional (3D) PhC have been designed and fabricated in which the width of the band gap can be manipulated by the modulation geometric parameters, *e.g.* lattice constant, filling factor, cladding material.

1D PhC is multilayer dielectric containing two different dielectric constant materials in periodic arrangement in one direction. Fiber Bragg gratings (FBGs) are spectral filters based on the principle of Bragg reflection, they typically reflect light over a narrow wavelength range and transmit all other wavelengths. FBGs have been widely used in optical fiber telecommunications [11] sensing applications [12], are a typical example for 1D PhC structure. 2D PhC is commonly fabricated by silicon-on-insulator (SOI) platform. Owing to the high refractive index difference between silicon layer where the devices are constructed and the buried oxide underneath, this platform enables strong light guiding performance [13, 14]. Nevertheless, in order to serve diverse applications, including all-optical signal processing and on-chip sensing [15], it is required to perform silicon hybrid integration to deal with some disadvantages of silicon. The drawbacks of silicon come from its intrinsic properties, such as bulk silicon has indirect bandgap, bulk silicon also does not possess second-order nonlinear susceptibility because of its centro-symmetric crystal structure, and the third-order nonlinear effects are hindered by two-photon absorption at telecommunication wavelength range. In order to achieve optical integrated functions, some “active” materials, *e.g.* polymers [16–19], graphene [20,21], carbon nanotubes (CNTs) [22–27], III/V compounds [28–30], quantum dots [31–33] have been integrated in/on silicon. Among those, semiconducting single-walled CNTs (s-SWNTs) have also drawn much attention because of their outstanding unique physical properties and chemical stability as well as nonlinear optical behavior [34–36]. Depending on the value of excitation energy, they can emit photoluminescence [37] accordingly, so s-SWNTs are potential for infrared light nano-emitters. They have been considered for optical sources [38,39], photodetectors [40], transistors [41] with the ambition to achieve minimizing opto-electronic devices.

In this work, we focus on photonic crystal silicon-based structures that are at the heart of nanophotonics to explore interesting applications such as light emission and sensing. We first report the 1D PhC sensor in Sec. II and then we present SOI slot PhC cavity towards light source application by integrating it with s-SWNTs in Sec. III. The conclusion is finally summarised.

II. 1D PHOTONIC CRYSTAL SENSOR

Figure 1(a) presents a typical structure of a common etched-FBG. It consists of the Bragg grating conducted in the fiber core with the refractive index n_c and coated by the fiber cladding with the refractive index of n_{cl} . The length of the Bragg grating is denoted with L_B . The radius of the fiber core is r_f . The difference between the refractive indices between the fiber core and cladding creates the mode confinement and normally this fundamental mode is not affected by the refractive index of surrounding medium. However, when the radius of the cladding materials reduces, the effective refractive index of the fundamental mode will depend on the surrounding material. The effective refractive index of the etched-FBG depends on the refractive index of the surrounding medium outside the fiber by a nonlinear behavior which causes a wavelength shift in the reflection. The value of the effective refractive index in an etched-FBG can be estimated by numerically solving the dispersion equation of a double-clad fiber model. The Bragg wavelength λ_B is determined from the FBG theory:

$$\lambda_B = n_{eff}\Lambda \tag{1}$$

in which n_{eff} is the effective refractive index and Λ is the periodic pitch or the grating period of the FBG.

The simulations show that the bandwidth and the intensity of the reflection peak of FBGs depend on the grating length and the change of the refractive index. Figure 1 (b) depicts the reflectance amplitude of a uniform etched-FBG with the following parameters: grating period $\Lambda = 0.5353 \mu\text{m}$, grating length $L_B = 4 \times 10^3 \mu\text{m}$, fiber core radius $r_f = 4.5 \mu\text{m}$, refractive index of fiber core $n_c = 1.45$, refractive index of fiber cladding $n_{cl} = 1.4464$, $\Delta n = 2.5 \times 10^{-4}$.

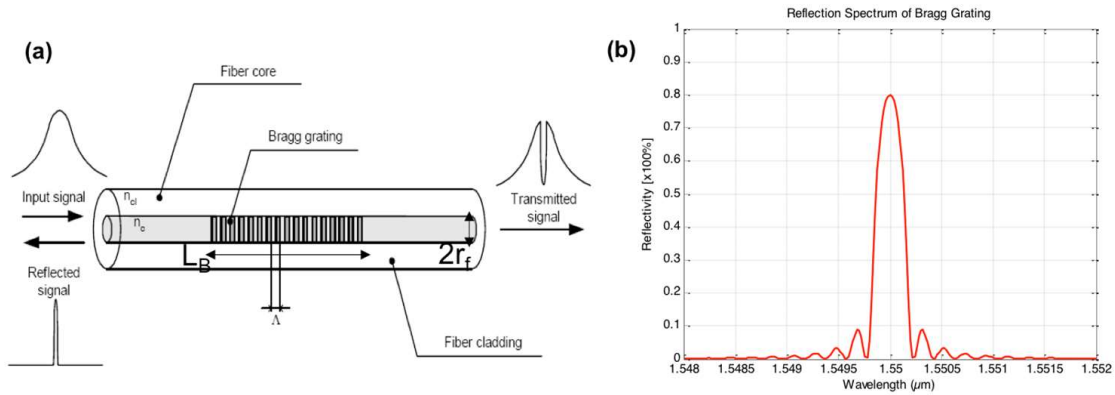


Fig. 1. (a) Schematic view of an etched-FBG, (b) Reflection spectrum of a typical etched-FBG.

The etched-FBGs were fabricated by holographic method in which a KrF-Excimer laser was used to excite the wavelength of 248 nm and Talbot interferometer. A commercial photosensitive germane-silicate single mode fiber was chosen as the optical fiber. The e-FBG was fabricated by wet chemical etching, the FBG region was dipped in hydrofluoric acid (HF) solution in order to increase the interaction of the propagating optical field inside the fiber core. Then the wavelength of the conducted FBG was ranging from 1530 nm to 1550 nm at room temperature and

the reflectivity was of 75–90% with FWHM of 0.15–0.30 nm and the etched-FBG length was of 15 mm.

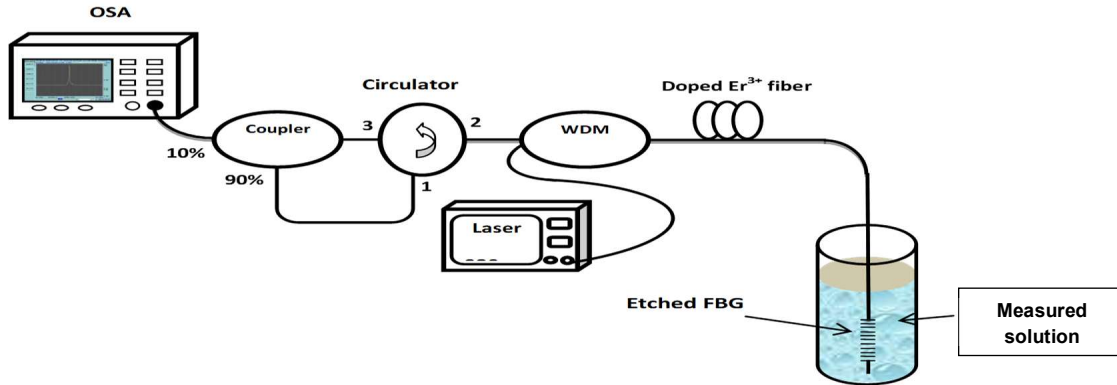


Fig. 2. Schematic diagram of the characterization setup of the proposed chemical sensor using 1D PhC on optical fiber integrated in fiber laser structure.

Figure 2 shows the characterization setup of the proposed chemical sensor based on 1D PhC (etched-FBG) on optical fiber sensor. The setup includes the resonator of the fiber laser. The resonator contains two mirrors, the first mirror was formed by a fiber-optic circulator. This fiber-optic circulator was utilized to couple light into the cavity. The 10/90 optical coupler helps to extract 10% of this coupled light to the performance system while 90% of the coupled light comes back to the cavity. The second mirror is the 1D PhC (etched-FBG) while the 3 m long erbium-doped silica fiber (Model: EDF-HCO-4000, Core-active, QC, Canada) acts as the optical gain medium. A 980 nm-laser diode is used to generate the optical pump with the output optical power of 100 mW in single-mode emission (SDLO-2560-172). The output light is then coupled to Er^{3+} doped silica fiber via a 980/1550 nm WDM to excite the Er^{3+} ions. The OSA is employed to monitor the spectra of the lasing emission. In the other end of the setup, the etched-FBG is immersed in the test solution. Here, nitrate solution with low concentration has been investigated. The nitrate is diluted in water with different nitrate concentration: 0, 10 ppm, 20 ppm, 30 ppm, 40 ppm, 50 ppm, 60 ppm, 70 ppm and 80 ppm.

The experimental results of the spectral response on nitrate concentration in water using 1D PhC on optical fiber sensor are shown in Figure 3.

Figure 3(a) reports the lasing spectral response of the 1D PhC on optical fiber as a function of the nitrate concentration in water. The optical power in dBm was collected by changing the nitrate concentration from 0 to 80 ppm, corresponds to curves 1 to 9. The experiments were carried out by using the OSA with the resolution of 0.01 nm hence the shifts of the peaks were clearly recognized. The obtained optical signal-to-noise ratio (OSNR) of this 1D PhC integrated Er^{3+} -doped fiber laser is higher than 40 dB and the spectra have the FWHM of 0.02 nm while the OSNR and the spectra are about 50 dB and 0.55 nm, respectively, when it is integrated with fiber laser. There is a red shift of 0.3 nm of the lasing spectra when the concentration of nitrate in water increases from 0 to 80 ppm. This wavelength shift is analysed by a linear fitting manner and corresponds to a sensitivity 3.5×10^{-3} nm/ppm and the limit of detection 3 ppm as shown in

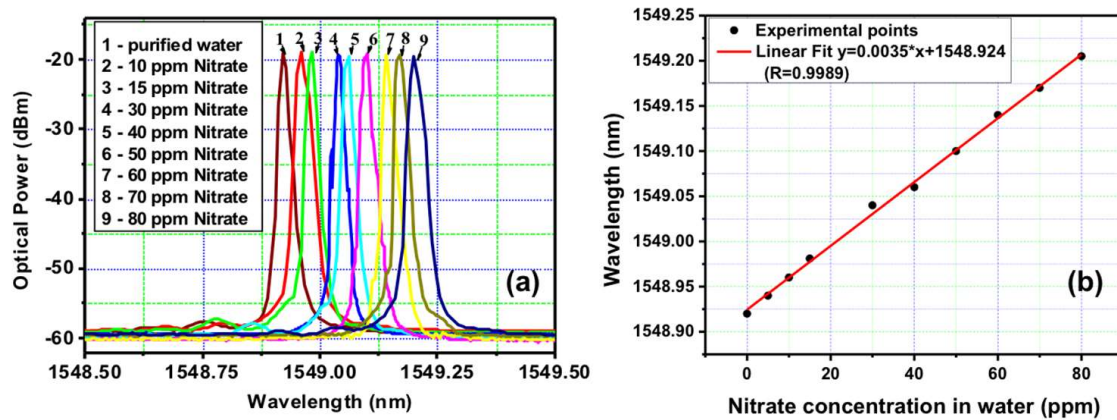


Fig. 3. (a) The spectral response collected from 1D PhC on optical fiber sensor as a function of nitrate concentration in water (curves 1 to 9); and (b) The experimental result and linear fitting behavior of Bragg wavelength when modifying the nitrate concentration in water from 0 to 80 ppm [42].

Figure 3(b). As this 1D PhC, *i.e.* etched-FBG integrated in fiber laser, possesses a narrow linewidth and high OSNR, the proposed chemical sensor can provide high accuracy and high sensitivity in chemical sensing by monitoring the shift of wavelength peak. Moreover, the collected optical intensity from the laser after a long length shows the potential for the contribution of this 1D PhC on optical fiber integrated in fiber laser structure on remote sensing applications.

III. PHOTOLUMINESCENCE ENHANCEMENT OF *s*-SWNTs IN SLOTTED SILICON 2D PHOTONIC CRYSTAL CAVITY

In this part, the particular behavior of the slotted silicon 2D PhC cavity is reported by demonstrating the photoluminescence enhancement of the *s*-SWNTs at around 1300 nm, showing the potentials for applications in producing on-chip nanosources. The slotted silicon 2D PhC cavity has the ability to confine light in an extremely tight region so it is considered as the nanoresonator. The cavity is conducted on a SOI wafer in which the silicon layer is of 220 nm thickness, the silica layer is around 2 μm onto the silicon substrate. The radius of the holes perforated in silicon background is around 105 nm. The approach is to modify the lattice constant in the light propagation with the length of the PhC region of about 60 μm . The mirrors are formed by adiabatically enlarging the longitudinal PhC lattice constant from 330 nm to 350 nm with the step size of 5 nm while maintaining the perpendicular one at 330 nm [43], a cladding material of 1.46 refractive index is considered in order to perform the hybrid integration with *s*-SWNTs solution. We also notice here that a 100 nm slot is introduced along the propagation direction with the purpose to enhance the interaction of light-material. This modification guarantees the transverse-electric (TE) polarized modes to be trapped in the center part of the PhC structure within a small mode volume and in a long time. The modes have been studied by 3D-finite-difference time-domain (3D-FDTD) method using Lumerical software before fabrication. The results show that two confined modes can be existed in this cavity. The first one is the fundamental TE-polarized mode with

the wavelength around $1.280 \mu\text{m}$ and the second mode has the resonance wavelength of about $1.271 \mu\text{m}$ as shown in Fig. 4. Fig. 4(a) presents the E_y component distribution of fundamental mode at 1284.34 nm with the Q -factor of around 21,000 in a mode volume of $0.024 (\lambda/n)^3$ while Fig. 4(b) provides the profile of the second mode with resonance wavelength at 1271.2 nm confined in a volume of $0.11 (\lambda/n)^3$ and the corresponding Q -factor is about 6000. Figures 4(c) and 4(d) present the Fourier transform of E_y component these two modes, which exhibit clearly the distribution of the mode in wavevector space. The two modes locate symmetrically outside the leaky area (the light cone is presented by the white circle).

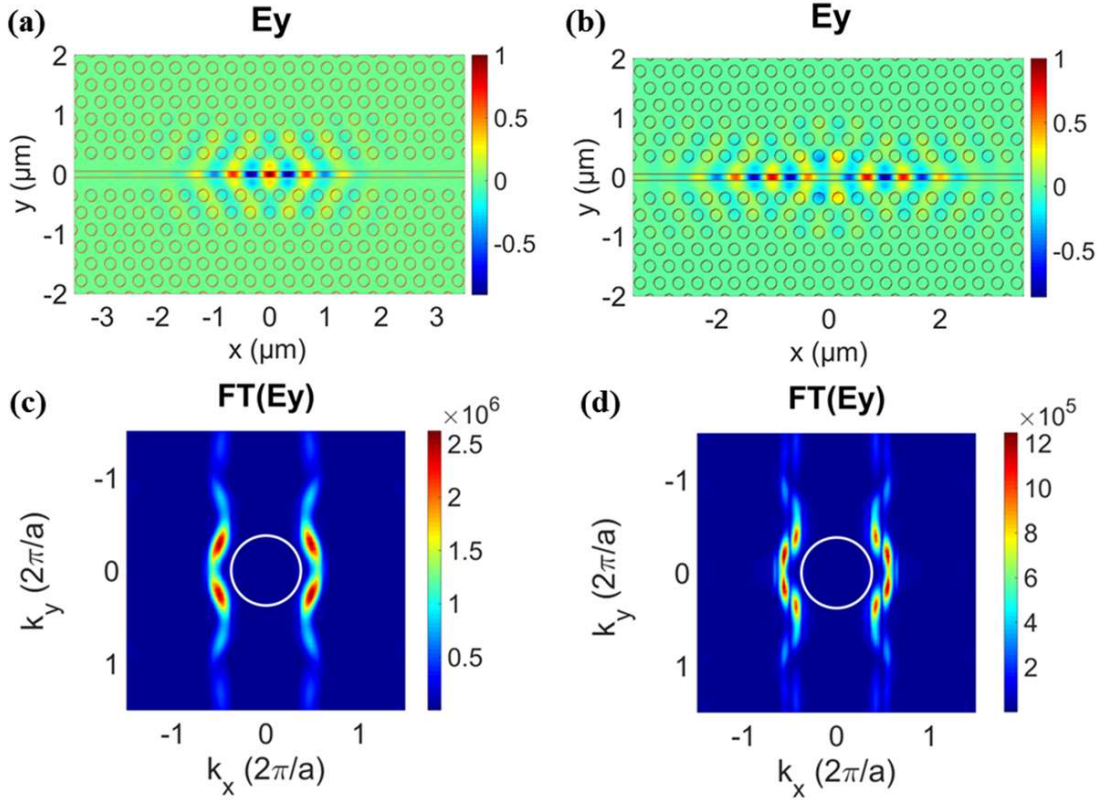


Fig. 4. The profile of E_y component of TE-like polarized resonance modes: (a) The fundamental mode at 1284.34 nm , (b) The second mode at 1271.2 nm , and Fourier transforms in wavevector space of the E_y component of these resonance modes are depicted in (c) and (d) in which the white circle presents the light cone.

As we can see from Fig. 4, the first confined mode is localized in the optical quantum well in the larger lattice constant region due to the fact that the smaller lattice constant the higher frequency level in the dispersion diagram. Whereas, the second mode expands broadly inside the barrier region. However, the mode is confined tightly inside the slot region, the fraction of the mode energy within the slot can be calculated up to 30%, that promotes strong light-matter interaction when infiltrating this cavity with s-SWNTs solution.

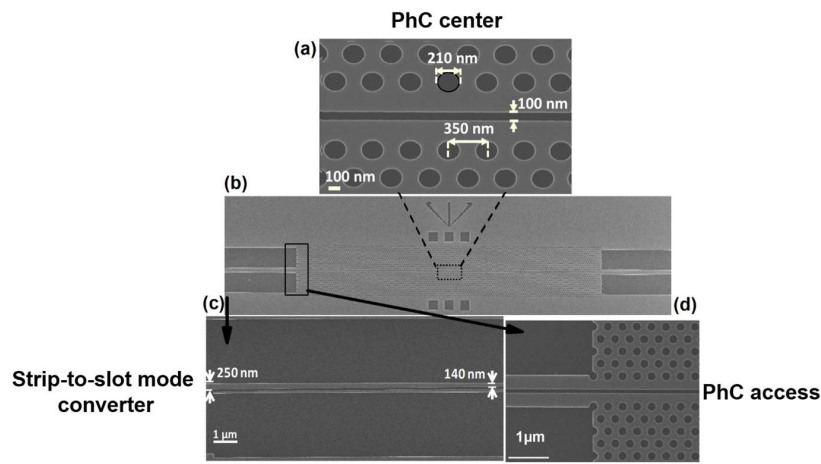


Fig. 5. Scanning electron microscope (SEM) images of fabricated slotted silicon 2D PhC cavity waveguide chip (a) Center PhC part, (b) Over view of the center part of the chip, (c) Strip-to-slot-mode converter working in 1300 nm region, (d) Transition part from the slotted silicon waveguide to slotted silicon 2D PhC cavity waveguide [43].

Figure 5 shows SEM images of the fabricated slotted 2D PhC cavity by electron beam lithography (Nanobeam NB-4 system, 80 kV) and dry etching (inductively coupled plasma with SF₆ gas). The complete chip consists of the PhC part (Fig. 5(a) and Fig. 5(b)) and the strip-to-slot mode converter (Fig. 5(c)) to properly propagate the mode from strip to slot fashion. The transition between silicon slot waveguide to PhC region is presented in Fig. 5(d). The quality of the fabrication process ensures the low insertion loss and efficient light injection from lensed fibers to the chip output in the total length of around 5 mm.

Figure 6(a) illustrates the schematic diagram of the photoluminescence (PL) setup of the s-SWNTs integration on the slotted silicon 2D PhC cavity. The s-SWNTs solution was prepared by using the polymer-sorting technique reported in [44]. A commercial dry SWNT powder (HiPCO from Unydim) was mixed with the polymer Poly-9,9-di-n-octyl-fluorenyl-2,7-diyl (PFO, Sigma-Aldrich) and toluene with the ratio of SWNT (5 mg): PFO (20 mg): toluene (30 ml). The mixture was homogenized by sonication. The supernatant solution was collected after 1 h of ultracentrifugation at 150,000 g. Fig. 6(b) depicts the PL behavior of the fabricated s-SWNTs. It is seen that the obtained solution contains only semiconducting type with the chirality of (8,6) and (8,7) [44]. In addition, the PL emission happens around 1280 nm for the (8,7) chirality s-SWNTs which matches well with the resonance wavelength of the cavity. In order to examine the PL characteristic of fabricated s-SWNTs, the purified SWNT solution was dropped onto the slotted 2D PhC silicon cavities and then annealing at 180°C in 15 mins in order to obtain the homogeneity of s-SWNTs onto the chip.

The PL spectra of the integrated system was collected by using the perpendicularly pumping beam from a Ti:sapphire laser (with a power of 2.6 mW) and an objective with 0.55 NA onto the top of the center chip, while the output signal was produced at the chip facet with a lensed fiber after a length of around 2500 μm as depicted in Fig. 6(a). A 320 mm spectrometer with a 950

lines/mm grating and nitrogen-cooled InGaAs photodetector array were utilized to analyse the collected signal. The experiments were carried out at room temperature. The excitation laser was tuned in the range of 710 nm to 780 nm covering the excitonic transition of s-SWNTs. The PL spectra of integrated system are shown in Fig. 6(c). We obtained two narrow linewidth peaks at the wavelength of 1271 nm and 1284 nm which correspond to the resonance modes of the slotted silicon 2D PhC cavity when it was pumped by the laser at 735 nm (red solid curve). Interestingly, the enhancement ratio of the PL can be estimated of around 1.15 between these two confined modes. The narrower FWHM of the peak at the fundamental mode compared with the second one can be explained by the difference of the Q -factor and mode volume of these modes as mentioned above. In here, the FWHM of the PL peak at 1284 nm is only around 0.34 nm, corresponding to a quality factor of around 4000.

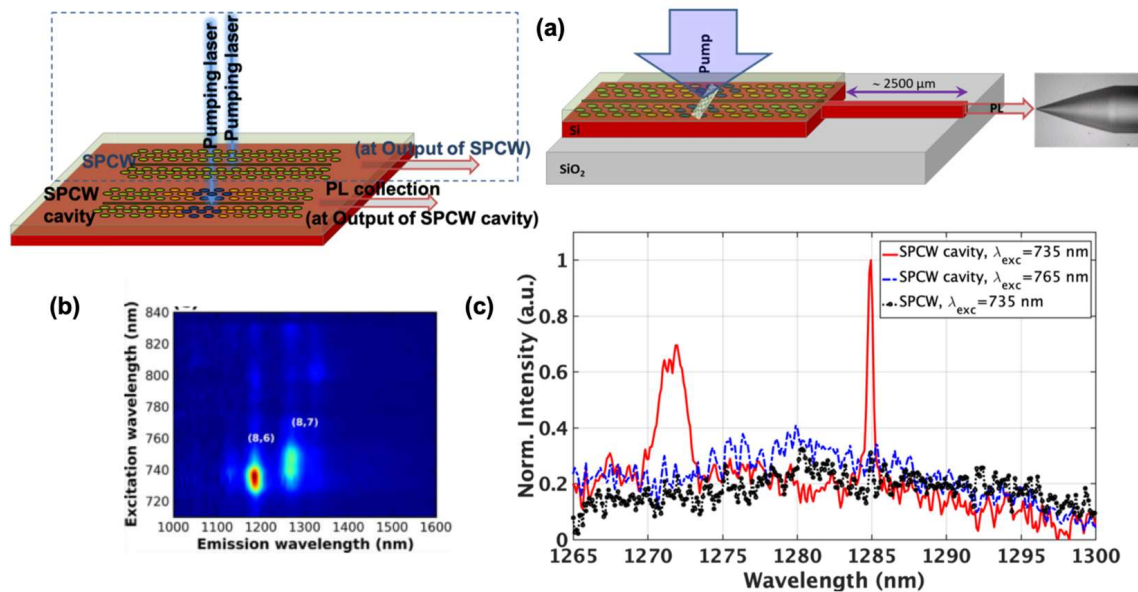


Fig. 6. (a) Illustration of PL characterization of the integrated system combining s-SWNTs and slotted silicon 2D PhC cavity waveguides, (b) PL spectra map of CNT solution with the excitation laser in the range of 710 nm - 840 nm, (c) PL spectra of the integrated system by pumping on the top of the system: the slotted silicon 2D PhC cavity at 735 nm (red line), at 765 nm (blue-dash-dot line), and on top of the slotted silicon 2D PhC waveguide at 735 nm (black-dot-circle line).

However, the PL enhancement of the s-SWNTs only occurs at the localized modes, as proved from the black-dot-circle line in Fig. 6(c). When the silicon 2D PhC waveguides were excited by the pumping laser at 735 nm, there is no PL enhancement. This PL enhancement of PL depends on the value of the excitation wavelength as shown in blue-dash-dot line in Fig. 6(c) in which the slotted silicon 2D PhC cavity was excited by 765 nm laser. These results exhibit the important role of the cavity as the nanoresonator to strengthen the light-matter interaction.

The strong interaction between the s-SWNTs and slotted silicon 2D PhC cavity is demonstrated by the enhancement of PL of the s-SWNTs. This initial result shows the potential to achieve nanosource which is mechanically robust with the SOI platform.

IV. CONCLUSION

We have demonstrated hybrid integrated nanophotonic silicon-based structures for chemical sensing and towards light nanosource applications. The 1D PhC sensor with achieved sensitivity of 3.2×10^{-3} nm/ppm and the LOD of 3 ppm, shows many advantages including high resolution for wavelength shift identification, high OSNR of about 50 dB, FWHM of 0.014 nm therefore enhancing its accuracy, precision and capability for remote sensing. In another scope, the hollow core SOI 2D PhC cavity waveguide integrated with s-SWNT has narrowband emission with the narrow FWHM of 0.34 nm. Interestingly, the PL enhancement for the two cavity modes differs 1.15 times between the two resonance modes. This result shows the potential to realize the nano on-chip source in silicon platform.

ACKNOWLEDGMENTS

This research is funded by Vietnam Academy of Science and Technology (VAST) under grant number “QTFR01.02/18-19”.

REFERENCES

- [1] M. Sieger, F. Balluff, X. Wang, S.-S. Kim, L. Leidner, G. Gauglitz, and B. Mizaikoff, *Anal. Chem.* **85** (2013) 3050.
- [2] H. Oda, A. Yamanaka, N. Ozaki, N. Ikeda, and Y. Sugimoto, *AIP Advances* **6** (2016) 065215.
- [3] G. Z. Mashanovich, F. Y. Gardes, D. J. Thomson, Y. Hu, K. Li, M. Nedeljkovic, J. Soler Penades, A. Z. Khokhar, C. J. Mitchell, and S. Stankovic, *IEEE J. Sel. Top. Quantum Electron.* **21** (2015) 407.
- [4] M. Loncar, T. Doll, J. Vuckovic, and Axel Scherer, *J. Light. Technol.* **18** (2000) 1402.
- [5] T. Tamura; K. Kondo; Y. Terada; Y. Hinakura; N. Ishikura; T. Baba, *J. Light. Technol.* **33** (2015) 3034.
- [6] S. Nur, H.-J. Lim, J. Elzerman, and J. J. L. Morton, *Appl. Phys. Lett.* **114** (2019) 091101.
- [7] J. J. D. Joannopoulos, S. Johnson, J. N. J. Winn, and R. R. D. Meade, *Photonic crystals: molding the flow of light*. 2008.
- [8] V. H. Pham, H. Bui, T. Van Nguyen, T. A. Nguyen, T. S. Pham, V. D. Pham, T. C. Tran, T. T. Hoang, and Q. M. Ngo, *Adv. Nat. Sci. Nanosci. Nanotechnol.* **7** (2016) 15003.
- [9] D. Dai, J. Wang, and Y. Shi, *Opt. Lett.* **38** (2013) 1422.
- [10] J. Wu; X. Yan; R. C. Watt; M. K. T. Nantel; L. Chrostowski; J. F. Young, “Widely Tunable, High-Q Two-Dimensional Photonic Crystal Cavities for cQED Applications,” 2018 IEEE Photonics Society Summer Topical Meeting Series (SUM), DOI: 10.1109/PHOSST.2018.8456716.
- [11] A. Balll, and W. W. Morey, *Opt. Lett.* **17** (1992) 420.
- [12] B. N. Shivananju, S. Yamdagni, R. Fazuldeen, A. K. Sarin Kumar, G. M. Hegde, M. M Varma, S. Asokan, *Rev. Sci. Instrum.* **84** (2013) 065002.
- [13] Y. A. Vlasov and S. J. Mcnab, *Opt. Express* **12** (2004) 1622.
- [14] Q. Xu, S. Manipatruni, B. Schmidt, J. Shakya, and M. Lipson, *Opt. Express* **15** (2007) 430.
- [15] E. Luan, H. Shoman, D. M. Ratner, K. C. Cheung, and L. Chrostowski, *Sensors* **18** (2019) 3519.
- [16] X. Zhang; A. Hosseini; X. Lin; H. Subbaraman; R. T. Chen, *J. Sel. Top. Quant.* **19** (2013) 3401115.
- [17] F. Qiu, H. Sato, A. M. Spring, D. Maeda, M. Ozawa, K. Odoi, I. Aoki, A. Otomo, and Yokoyama, *Appl. Phys. Lett.* **107** (2015) 123302.
- [18] Z. Huang, Q. Huang, Y. Wang, and J. Xia, *Opt. Eng.* **57** (2018) 046108.
- [19] T. J. Duffin, M. P. Nielsen, F. Diaz, S. Palomba, S. A. Maier, and R. F. Oulton, *Opt. Lett.* **41** (2016) 155.

- [20] S. M. Hussein, I. F. Crowe, N. Clark, M. Milosevic, A. Vijayaraghavan, F. Y. Gardes, G. Z. Mashanovich, and M. P. Halsall, *Nanoscale Res. Lett.* **12** (2017) 600.
- [21] L. A. Shiramin, W. Xie, B. Snyder, P. D. Heyn, P. Verheyen, G. Roelkens, and D. V. Thourhout, *IEEE Photon. Tech. L.* **30** (2018) 157.
- [22] A. Eatemadi, H. Daraee, H. Karimkhanloo, M. Kouhi, N. Zarghami, A. Akbarzadeh, M. Abasi, Y. Hanifehpour, and S. W. Joo, *Nanoscale Res. Lett.* **9** (2014) 393.
- [23] S. Khasminskaya, F. Pyatkov, B. S. Flavel, W. H. Pernice, and R. Krupke, *Adv. Mater.* **26** (2014) 3465.
- [24] X. He, H. Htoon, S. K. Doorn, W. H. P. Pernice, F. Pyatkov, R. Krupke, A. Jeantet, Y. Chassagneux, and C. Voisin, *Nat. Mater.* **17** (2018) 663.
- [25] E. Durán-Valdeiglesias, W. Zhang, C. Alonso-Ramos, S. Serna, X. Le Roux, D. Maris-Morini, N. Caselli, F. Biccari, M. Gurioli, A. Filoramo, E. Cassan, and L. Vivien, *Sci. Rep.* **8** (2018) 11252.
- [26] K. Liu, and V. J. Sorger, *Opt. Mater. Express* **5** (2015) 1910.
- [27] F. Pyatkov, V. Fütterling, S. Khasminskaya, B. S. Flavel, F. Hennrich, M. M. Kappes, R. Krupke, and W. H. P. Pernice, *Nat. Photonics* **10** (2016) 420.
- [28] M. Hopkinson, T. Martin, and P. Smowton, *Semicond. Sci. Tech.* **28** (2013) 090301.
- [29] G. de Valicourt, C.-M. Chang, M. S. Eggleston, A. Melikyan, C. Zhu, J. Lee, J. E. Simsarian, S. Chandrasekhar, J. H. Sinsky, K. W. Kim, P. Dong, A. Maho, A. Verdier, R. Brenot, and Y. K. Chen, *J. Light. Technol.* **36** (2018) 265.
- [30] S. Cheung, Y. Kawakita, Kuanping Shang, and S. J. Ben Yoo, *Opt. Express* **23** (2015) 22431.
- [31] C. Zeng, Y. Ma, Y. Zhang, D. Li, Z. Huang, Y. Wang, Q. Huang, J. Li, Z. Zhong, J. Yu, Z. Jiang, and J. Xia, *Opt. Express* **23** (2015) 22250.
- [32] I. J. Luxmoore, R. Toro, O. Del Pozo-Zamudio, N. A. Wasley, E. A. Chekhovich, A. M. Sanchez, R. Beanland, A. M. Fox, M. S. Skolnick, H. Y. Liu, and A. I. Tartakovskii, *Sci. Rep.* **3** (2013) 1239.
- [33] M. Davanco, J. Liu, L. Sapienza, C.-Z. Zhang, J. V. De Miranda Cardoso, V. Verma, R. Mirin, S. W. Nam, L. Liu, and K. Srinivasan, *Nat. Commun.* **8** (2017) 889.
- [34] R. Jansen and P. Wallis, "Manufacturing, *Mater. Matters* **4** (2009) 23.
- [35] R. Martel, V. Derycke, C. Lavoie, J. Appenzeller, K. Chan, J. Tersoff, P. Avouris, *Phys. Rev. Lett.* **87** (2001) 256805.
- [36] S. M. Bachilo, M. S. Strano, C. Kittrell, R. H. Hauge, R. E. Smalley, and R. B. Weisman, *Science* **298** (2002) 2361.
- [37] E. Gauffrès, N. Izard, L. Vivien, S. Kazaoui, D. Marris-Morini, and E. Cassan, *Opt. Lett.* **34** (2009) 3845.
- [38] S. Wang, Q. Zeng, L. Yang, Z. Zhang, Z. Wang, T. Pei, L. Ding, X. Liang, M. Gao, Y. Li, and Lian-Mao Peng, *Nano. Lett.* **11** (2011) 23.
- [39] X. He, H. Htoon, S. K. Doorn, W. H. P. Pernice, F. Pyatkov, R. Krupke, A. Jeantet, Y. Chassagneux, and C. Voisin, *Nat. Mat.* **17** (2018) 663.
- [40] M. Freitag, Y. Martin, J. A. Misewich, R. Martel, and P. Avouris, *Nano Lett.* **3** (2003) 1067.
- [41] N. Izard, S. Kazaoui, K. Hata, T. Okazaki, T. Saito, S. Iijima, and N. Minami, *Appl. Phys. Lett.* **92** (2008) 243112.
- [42] T. B. Pham, H. T. Le, H. Bui, and V. H. Pham, *Sensors* **17** (2017) 7.
- [43] T. H. C. Hoang, W. Zhang, S. F. Serna, C. Caer, X. Le-Roux, L. Vivien, and E. Cassan, *IEEE Photon. Tech. Lett.* **27** (2015) 2138.
- [44] F. La China, N. Caselli, F. Sarti, F. Biccari, U. Torrini, F. Intonti, A. Vinattieri, E. Durán-Valdeiglesias, C. Alonso-Ramos, X. Le Roux, M. Balestrieri, A. Filoramo, L. Vivien, and M. Gurioli, *J. Appl. Phys.* **120** (2016) 123110.